Physics – Uspekhi **52** (1) 79 – 92 (2009)

METHODOLOGICAL NOTES PACS numbers: **66.20. – d**, **91.35. – x**, **93.85. – q**

Direct observations of the viscosity of Earth's outer core and extrapolation of measurements of the viscosity of liquid iron

D E Smylie, V V Brazhkin, A Palmer

DOI: 10.3367/UFNe.0179.200901d.0091

Contents

From the Editorial Board. Problems of geophysics are not found among the topics which *Uspekhi Fizicheskikh Nauk* (*Physics – Uspekhi*) can elucidate at regular intervals and devote an appreciable part of its pages to them. Basically, physics make a close study of simple objects based on data from well-reproduced experiments and reliable theoretical models. On the contrary, the Earth constitutes a very complex object. Information about its internal structure is extracted from observational results whose interpretation directly depends on the adopted model and the validity of the latter in the case of a complex system is far from being apparent. At the same time, the geophysical matters (Earth's structure and its evolution, catastrophic event forecast, to name but a few) pique active interest in all of us. Publishing this article and related discussion we formed the intention to acquaint the readers of *Uspekhi Fizicheskikh Nauk* (*Physics – Uspekhi*) with one of the topical problems of geophysics and to lay emphasis (using the estimate of Earth's liquid core viscosity as an example) on both the complexity of the subject and the lack of the generally accepted viewpoint even among the leaders in the field). At the present time we consider the discussion terminated. The Editorial Board of *Uspekhi Fizicheskikh Nauk* (*Physics – Uspekhi*) has no intention of publishing the papers on this theme in the nearest future.

D E Smylie Department of Earth and Space Science and Engineering, York University,
4700 Keele Street, Toronto, Ontario, M3J 1P3, Canada
Tel. (416) 736-2100, ext. 66438. Fax (416) 736-5817
E-mail: doug@core.yorku.ca
V V Brazhkin L F Vereshchagin Institute for High Pressure Physics, Russian Academy of Sciences,
142190 Troitsk, Moscow region, Russian Federation
Tel. (7-495) 751 00 11. Fax (7-495) 751 00 12
E-mail: brazhkin@hppi.troitsk.ru
A Palmer Sander Geophysics Ltd., 260 Hunt Club Road, Ottawa, Ontario, K2P 1K2, Canada. E-mail: palmer@core.yorku.ca

Received 16 January 2008, revised 4 August 2008
Uspekhi Fizicheskikh Nauk **179** (1) 91 – 105 (2009)
DOI: 10.3367/UFNr.0179.200901d.0091
Translated by V V Brazhkin; edited by A Radzig

Abstract. Estimates vary widely as to the viscosity of Earth's outer fluid core. Directly observed viscosity is usually orders of magnitude higher than the values extrapolated from high-pressure high-temperature laboratory experiments, which are close to those for liquid iron at atmospheric pressure. It turned out that this discrepancy can be removed by extrapolating via the widely known Arrhenius activation model modified by lifting the commonly used assumption of pressure-independent activation volume (which is possible due to the discovery that at high pressures the activation volume increases strongly with pressure, resulting in 10^2 Pa s at the top of the fluid core, and in 10^{11} Pa s at its bottom). There are of course many uncertainties affecting this extrapolation process. This paper reviews two viscosity determination methods, one for the top and the other for the bottom of the outer core, the former of which relies on the decay of free core nutations and yields 2371 ± 1530 Pa s, while the other relies on the reduction in the rotational splitting of the two equatorial translational modes of the solid inner core oscillations and yields an average of $1.247 \pm 0.035 \times 10^{11}$ Pa s. Encouraged by the good performance of the Arrhenius extrapolation, a differential form of the Arrhenius activation model is used to interpolate along the melting temperature curve and to find the viscosity profile across the entire outer core. The viscosity variation is found to be nearly log-linear between the measured boundary values.

1. Introduction

The properties of Earth's deep interior, such as its elasticity, density, pressure, and gravity, have traditionally been obtained through the inversion of seismic observations. While these have been important to our understanding of Earth's internal structure, the viscosity of the outer fluid core is crucial to our understanding of its dynamics and the generation of the geomagnetic field. Estimates of the viscosity of Earth's outer fluid core range over many orders

of magnitude [1]. Direct observations and limits on viscosity have traditionally been much larger [2, 3] than the values determined by most theoretical estimates [4–7], as well as from extrapolations of high-pressure–high-temperature experiments [8–13]. The extent of this dichotomy is well illustrated in the handbook tabulation of viscosity by Secco [14]. He divides viscosity estimates into several categories: those derived from geodetic studies which range as high as 10^{11} Pa s, those derived from short-period seismological studies which range as high as 8.6×10^{11} Pa s, those derived from magnetic field studies which range as high as 2.7×10^{7} Pa s, and those derived from the theory of liquid metals which range between 2.5×10^{-3} Pa s and 50 Pa s. The gap between observation and theory ranges beyond fourteen orders of magnitude!

A departure from the improbably small values of viscosity obtained by extrapolations of laboratory studies was found [15, 16] on the basis of the Arrhenius activation model. Although this model was widely used [13, 17], it had been assumed that the activation volume was not strongly pressure-dependent. From measurements of the average size of crystallites in iron samples rapidly quenched from melts, and from analysis of the data for molecular liquids, it was revealed [15, 16] that the activation volume is pressure-dependent, leading to viscosity estimates close to 10^{2} Pa s at the top of the liquid core, increasing by nine orders of magnitude to 10^{11} Pa s at the bottom, *although, it should be emphasized that the uncertainties in the extrapolations are very large*.

Unusual properties of the lower outer core have long been suspected, going back to the 1926 claim by Jeffreys [18] of a strong negative P-wave velocity gradient there. While the P gradient is now thought to be small, but slightly positive, possibly due to solid inclusions slowing compressional waves in that region [19], its properties remain a subject of speculation. A new seismic phase, PKhKP, has even been suggested by Bullen and Bolt [20] as originating from reflections in the lower outer core. In this article we review two direct methods of measuring the viscosity of the outer core: one giving measurements of the viscosity at the top, the other giving measurements at the bottom. They both closely confirm the boundary values derived from the Arrhenius extrapolations [15, 16].

The outer fluid core is capable of a free motion, in which it rotates about an axis different compared to the rest of the Earth, called the free core nutation (FCN). In the initial study of this phenomena by Poincaré [21], the fluid core was assumed to be incompressible, uniform, and non-self-gravitating, with no inner body, and enclosed by a rigid mantle and crust. This model gave a large, long-period retrograde free core nutation (RFCN) and an associated nearly diurnal free, retrograde wobble (NDFW). The ratio of the nutation period to the wobble period is close to the ratio of the amplitude of the nutation to the wobble amplitude. While the Poincaré model has been beautifully confirmed by laboratory models of contained rotating fluids in which the rotation of the container is constrained [22], its relevance to the real Earth, in which the rotation of the container is unconstrained, there is an inner body, the fluid is compressible, stratified, and self-gravitating, and the boundaries are deformable, does not appear to be direct. The governing equation then becomes the subseismic wave equation rather than the inertial wave equation [23]. The free core nutations are solutions of the subseismic wave equation, which are close to pure rotations with respect to the shell (mantle plus crust), though not exactly so [24–26]. Thus, motions in the Earth frame of reference imitate the 'spin-over' mode of the inertial wave equation. Some of the basic features of the Ekman layers at the two boundaries in the real Earth resemble those of the spin-over mode but previous theories were not given in detail, with only results shown, possibly due to Greenspan's dictum that the "computation of viscous effects, ..., is laborious but straightforward" [27]. We give below full details of the analysis of the Ekman layers at the two boundaries, which is independent of the inertial wave equation, and calculate in detail the viscous coupling between the outer and inner cores and the shell in two Appendices (A and B). These details appear not to have been published previously. Explicit expressions were obtained for the reciprocal Q's at both boundaries, and for the viscous coupling torques between the outer core and the shell, and between the outer and inner cores. The inner core is found to be tightly coupled by viscosity to the outer core in the free core nutations.

The outer core is also the seat of the generation of the main magnetic field and electromagnetic effects need to be considered. For motions with wavelengths that are large compared to the electromagnetic skin depth, core oscillations can be treated as a purely mechanical phenomenon [28, 29]. Scaling arguments show that for such motions the Lorentz force density is many orders of magnitude smaller than the dominant Coriolis acceleration [30]. Similarly, electromagnetic coupling appears to be extremely weak [31, 32]. Nonetheless, Buffett et al. [33] have argued that it may be important in exciting and damping the free core nutations. They invoke a highly conducting layer 200 m thick in the lower mantle, with a conductivity of 5×10^{5} S m^{-1}, in contrast to the usually assumed value of 100 S m^{-1}. Such a large increase in conductivity would screen out the observed secular variation, as originally pointed out by Runcorn [34] (treated in more detail in paper [35]). The cut-off time constant is controlled by the root-mean-square conductivity [36], and the 200-m thick layer with a conductance of 10^{8} S would completely screen out the secular variation.

The variational calculations by Jiang [24] of wobble-nutation modes in realistic Earth models using bicubic splines as support functions led to the discovery of a second prograde free core nutation (PFCN), in addition to the classical RFCN described by Poincaré. In the Earth frame, only a slight perturbation in the NDFW period results in a PFCN, and presumably this is due to Coriolis splitting in the rotational deformation of the shell. This second mode had already been found in studies of the response of the Earth to nutational forcing [37, 38]. At the time, the very long baseline interferometric (VLBI) record of nutation observations was too short to give an acceptable confidence level, and no claim of observational support was made.

More recently, VLBI nutation series from the Goddard Space Flight Center (GSFC) and the United States Naval Observatory (USNO), both in excess of twenty-three years in length, were analyzed [39]. Both the RFCN and the PFCN were found to be closely in free decay. As many as fourteen successive spectral estimates down the time axis were used to investigate the decay rates and, together with Ekman layer analysis at both boundaries, they were found to yield a mean value of 2.371 ± 1.530 Pa s for the recovered viscosity at the top of the outer core, slightly higher than the extrapolated

value [15, 16] but much smaller than the average value for the core evaluated by Davis and Whaler [3].

A second set of direct measures of the viscosity of the outer fluid core derives from studies of the free translational modes of oscillation of the solid inner core, which yield values at the bottom. The solid inner core at its surface is about 1.2×10^3 kg m^{-3} denser than the surrounding fluid. It is held in its central position by relatively weak gravitational forces and is capable of executing free translational oscillations or pendulum motions. These motions were first discussed by Louis Slichter [40] and are sometimes referred to as Slichter modes. Because of Earth's rotation, they are split by the Coriolis acceleration into three distinct modes: one up and down the rotation axis, one prograde in the equatorial plane, and one retrograde in the equatorial plane. Analysis of many long records of superconducting gravimeter observations around the globe [41–43] gives periods of 3.5822 ± 0.0012 h for the retrograde equatorial mode, 3.7656 ± 0.0015 h for the axial mode, and 4.0150 ± 0.0010 h for the prograde equatorial mode. The rotational splitting of the two equatorial modes is reduced by viscosity, while the axial mode is not much affected. Two measures of viscosity result. The reduction in splitting of the retrograde equatorial mode gives $1.190 \pm 0.035 \times 10^{11}$ Pa s, while the reduction in splitting of the prograde equatorial mode gives $1.304 \pm 0.034 \times 10^{11}$ Pa s, with an average value reaching $1.247 \pm 0.035 \times 10^{11}$ Pa s. Given the range of past differences between extrapolations of laboratory measurements and direct observations of outer core viscosity, this confirmation of the Arrhenius extrapolations [15, 16] is truly remarkable.

2. Viscosity at the top of the outer core

In realistic Earth models, the finite element-based variational calculations of Jiang [24] revealed that there are two free core nutations. In addition to the classical retrograde mode (RFCN), a second prograde mode (PFCN) appears. The motions are illustrated by Poinsot constructions in which a small body cone rolls once per sidereal day without slipping on a large space cone as shown in Fig. 1.

In the Earth frame, both modes appear as nearly diurnal retrograde wobbles, the wobble associated with the RFCN being a little faster than retrograde diurnal, while the wobble associated with the PFCN is a little slower. For the RFCN, the ratio of the nutation amplitude a_N to the wobble amplitude a_W is given by $a_N/a_W - 1 = -\Omega/\sigma_N$, where Ω is Earth's angular rotation velocity, and σ_N is the nutation angular frequency. For the PFCN, the ratio is defined by $a_N/a_W + 1 = \Omega/\sigma_N$.

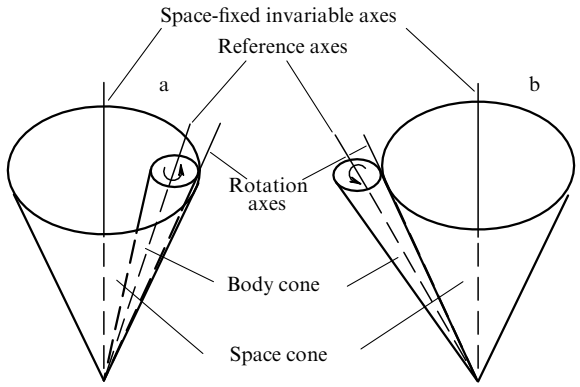

Figure 1. Poinsot constructions for free core nutations. The RFCN is shown on the left (a), and the PFCN on the right (b). In each mode, the small body cone rolls once per sidereal day without slipping on the large space cone. The line of cone contact is Earth's instantaneous rotation axis.

In the study [39], both the RFCN and the PFCN were found to be in free decay, on the basis of VLBI nutation measurement series from GSFC and the USNO in excess of twenty-three years. The GSFC series ran from August 3, 1979 to March 6, 2003 and spanned a period of 8,617 days, while the USNO series ran from August 3, 1979 to March 29, 2003 and spanned 8,631 days. In order to investigate the decays in detail, each record was divided into 2,000-day segments advancing down the time axis in 400-day steps. Spectral densities were estimated on the basis of each of four successive 2000-day segments. The result was spectral estimates centered at 1,600 days into the record, and at 400 day increments down the time axis thereafter. The spectral amplitudes are shown plotted against time in Fig. 2.

In free decay, the logarithm of the nutation amplitude a_N decreases linearly with time as

$$\log a_N = ct + d, \tag{1}$$

with

$$c = \pm\frac{\pi \log e}{Q_N T_N} = -\frac{\log e}{\tau}, \qquad d = \log a_{N_0}, \tag{2}$$

$$t_{1/2} = \tau \ln 2, \tag{3}$$

where T_N is the signed nutation period (negative for retrograde, positive for prograde), Q_N is the apparent Q of the nutation in the space frame, a_{N_0} is the amplitude at time $t = 0$, τ is the e-folding time, and $t_{1/2}$ is the half-life of the decay. The upper positive sign applies to the RFCN, while the lower negative sign to the PFCN.

The actual physical dissipation takes place in the Earth frame, through the associated nearly diurnal retrograde wobbles, and is measured by Q_W. Q_W is related to the apparent nutation Q_N by the expression

$$Q_W = \pm\left(1 - \frac{T_N}{T_s}\right) Q_N, \tag{4}$$

with T_s being the length of the sidereal day. The wobble Q is defined by the formula

$$Q_W = -\frac{\pi \log e}{c T_s}\left(1 - \frac{T_s}{T_N}\right). \tag{5}$$

Results of the regression on the logarithm of the nutation amplitude (1) are listed in Table 1.

In realistic Earth models, the two free core nutations have associated nearly diurnal retrograde wobbles that are close to pure rotations with respect to the shell (mantle and crust) and the inner core [24–26]. Their angular frequencies approach $-\Omega$, the negative of Earth's angular rotation velocity. In spherical polar coordinates (r, θ, ϕ), the velocity field is close to

$$\mathbf{v} = -\boldsymbol{\theta} Ar \sin(\phi + \Omega t) - \boldsymbol{\phi} Ar \cos\theta \cos(\phi + \Omega t) \tag{6}$$

for nearly diurnal wobbles with the amplitude A.

On the assumption that the boundary layers are a small fraction of the radius in thickness, the leading order boundary

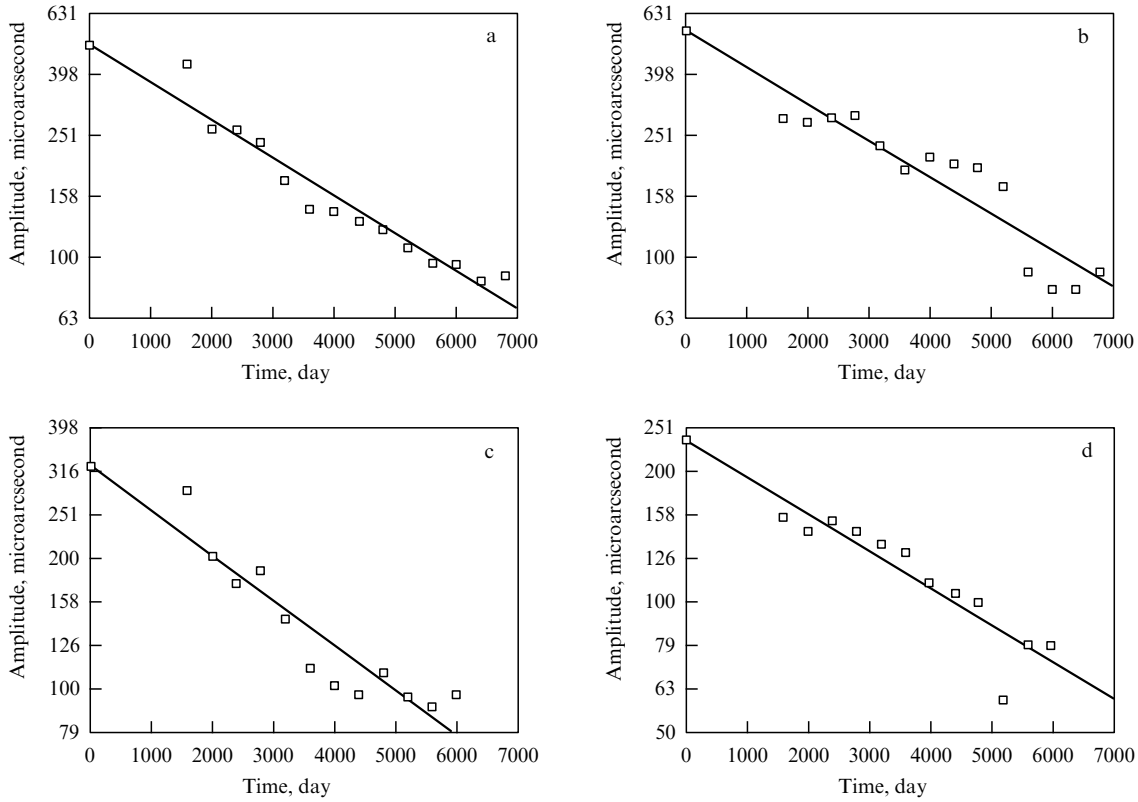

Figure 2. Amplitudes of the free core nutations plotted on a logarithmic scale as functions of time. Upper plots show the RFCN: upper left for GSFC (a), and upper right for USNO (b); lower plots show the PFCN: lower left for GSFC (c), and lower right for USNO (d). Linear fits to the time dependences are shown directly on the plots, along with extrapolated values at the time origin.

Table 1. Fitted decay parameters of the free core nutations.

		c, 10^{-4} day^{-1}	d	a_{N_0}, μas	T_N, day	Q_N	Q_W	$t_{1/2}$, day
RFCN	GSFC	−1.23909 ±0.1006	2.69740	498.20	−440.865 ±31.519	26.404 ±4.031	11.068 ±2.481	2429
	USNO	−1.20360 ±0.1486	2.74547	556.51	−410.147 ±17.706	27.444 ±4.573	11.394 ±2.390	2501
PFCN	GSFC	−1.03217 ±0.1461	2.51192	325.03	474.308 ±86.578	34.052 ±11.036	13.221 ±6.698	2916
	USNO	−0.85237 ±0.1236	2.37147	235.22	444.847 ±74.677	41.356 ±12.939	16.009 ±7.696	3532

layer equations in the (θ, ϕ) components of the extra boundary layer velocity, (v_θ, v_ϕ), are as follows [44, 45]

$$\frac{\partial v_\theta}{\partial t} - 2\Omega v_\phi \cos\theta = \nu \frac{\partial^2 v_\theta}{\partial r^2}\,, \qquad \frac{\partial v_\phi}{\partial t} + 2\Omega v_\theta \cos\theta = \nu \frac{\partial^2 v_\phi}{\partial r^2}\,, \tag{7}$$

with ν denoting the kinematic viscosity.

The detailed solution of these boundary layer equations and the calculation of the rates of energy dissipation in each of the respective layers at the boundaries of the outer core is left to Appendix A. From equation (85) (see Appendix A), the rate of energy dissipation in each of the respective boundary layers is equal to

$$\frac{\mathrm{d}E}{\mathrm{d}t} = \frac{\pi}{35}\,\rho_0 A^2 r_0^4 \sqrt{2\nu\Omega}\,\left(9\sqrt{3}+19\right), \tag{8}$$

with ρ_0 denoting the density, A the amplitude, and r_0 the radius at the boundaries. If A_a is the amplitude of the nearly diurnal retrograde wobble of the outer core with respect to the inner core, and if A_b is the appropriate amplitude with respect to the shell, the total energy dissipated per cycle in both boundary layers is written out as

$$E = \frac{2\pi}{\Omega}\frac{\mathrm{d}E}{\mathrm{d}t} = \frac{2}{35}\,\pi^2\left(\rho_0(a) A_a^2 a^4 \sqrt{\nu_a} + \rho_0(b) A_b^2 b^4 \sqrt{\nu_b}\right) \times \sqrt{\frac{2}{\Omega}}\left(9\sqrt{3}+19\right), \tag{9}$$

with $\rho_0(a)$ and ν_a representing the density and kinematic viscosity just outside the inner core boundary (ICB) (at $r_0 = a$), and $\rho_0(b)$ and ν_b representing the density and kinematic viscosity just inside the core–mantle boundary (CMB) (at $r_0 = b$). The quality factor Q_W of the nearly diurnal wobbles accompanying the free core nutations is defined as 2π times the ratio of the total energy to the energy

E dissipated per cycle. The total energy of the motion is close to

$$\frac{1}{2}\, I_{\rm oc} A^2\,, \tag{10}$$

where $I_{\rm oc} = 911.79 \times 10^{34}$ kg m^2 is the moment of inertia of the outer core. The reciprocal of the overall quality factor is then the sum of the reciprocals of the effective quality factors at the two boundaries, namely

$$\frac{1}{Q_{\rm W}} = \frac{1}{Q_a} + \frac{1}{Q_b}\,, \tag{11}$$

$$\frac{1}{Q_a} = \frac{2\pi\rho_0(a)a^4\sqrt{2\nu_a/\Omega}\,\left(9\sqrt{3}+19\right)}{35 I_{\rm oc}}\,, \tag{12}$$

$$\frac{1}{Q_b} = \frac{2\pi\rho_0(b)b^4\sqrt{2\nu_b/\Omega}\,\left(9\sqrt{3}+19\right)}{35 I_{\rm oc}}\,. \tag{13}$$

Neglecting the perturbation of shell rotation and denoting the amplitude of the nearly diurnal wobble of the outer core by B and that of the inner core by C, one finds

$$A_b = B\,, \qquad A_a = B - C\,.$$

The detailed calculation of the viscous coupling torques that the outer core exerts on the shell and inner core is left to Appendix B. From expressions (103) and (104) derived there for the constants γ_a and γ_b, and ignoring the small Chandler resonance effect, the equation of motion of the outer core acquires the form

$$\begin{aligned}&\gamma_a \exp\left(-{\rm i}\Omega t\right)(C-B) - \gamma_b \exp\left(-{\rm i}\Omega t\right) B\\ &\quad = I_{\rm oc}(\dot{B} - {\rm i}\Omega B)\exp\left(-{\rm i}\Omega t\right),\end{aligned} \tag{14}$$

while that of the inner core is

$$-\gamma_a \exp\left(-{\rm i}\Omega t\right)(C-B) = I_{\rm ic}(\dot{C} - {\rm i}\Omega C)\exp\left(-{\rm i}\Omega t\right), \tag{15}$$

with $I_{\rm ic}$ representing the moment of inertia of the inner core. Equations (14) and (15) constitute a linear, homogeneous differential system. For time dependence $\exp(\lambda t)$, it becomes

$$\begin{pmatrix} \lambda - {\rm i}\Omega + \dfrac{\gamma_a+\gamma_b}{I_{\rm oc}} & -\dfrac{\gamma_a}{I_{\rm oc}} \\ -\dfrac{\gamma_a}{I_{\rm ic}} & \lambda - {\rm i}\Omega + \dfrac{\gamma_a}{I_{\rm ic}} \end{pmatrix} \begin{pmatrix} B \\ C \end{pmatrix} = 0 \tag{16}$$

with the characteristic equation

$$\lambda'^2 + \left(\frac{1+\gamma_b/\gamma_a}{I_{\rm oc}} + \frac{1}{I_{\rm ic}}\right)\gamma_a \lambda' + \frac{\gamma_a\gamma_b}{I_{\rm oc} I_{\rm ic}} = 0\,, \tag{17}$$

where $\lambda' = \lambda - {\rm i}\Omega$.

From expressions (103), (104) follows the ratio

$$\frac{\gamma_b}{\gamma_a} = \frac{\rho_0(b)b^4\sqrt{\nu_b}}{\rho_0(a)a^4\sqrt{\nu_a}} = \frac{1}{117.4} \tag{18}$$

that would hold for the density ratio of 0.8069, radius ratio of 2.8668, and the ratio of the square roots of the kinematic viscosities equal to 1/6400. Correct to terms of first order in the small quantity γ_b/γ_a, the roots of the characteristic equation are given by

$$\lambda'_1 = \frac{\gamma_b}{I_{\rm c}}\,, \qquad \lambda'_2 = -\frac{I_{\rm c}}{I_{\rm oc} I_{\rm ic}}\,\gamma_a - \frac{I_{\rm ic}}{I_{\rm oc} I_{\rm c}}\,\gamma_b\,, \tag{19}$$

with $I_{\rm c} = I_{\rm oc} + I_{\rm ic}$ representing the moment of inertia of the entire core. The admissible solutions of system (16) are then the following linear combinations

$$\begin{aligned} B\exp\left(-{\rm i}\Omega t\right) &= \alpha\exp\left(\lambda'_1 t\right) + \beta\exp\left(\lambda'_2 t\right),\\ C\exp\left(-{\rm i}\Omega t\right) &= \left(1 + \frac{\gamma_b}{\gamma_a}\,\frac{I_{\rm ic}}{I_{\rm c}}\right)\alpha\exp\left(\lambda'_1 t\right)\\ &\quad - \left(\frac{I_{\rm oc}}{I_{\rm ic}} - \frac{\gamma_b}{\gamma_a}\,\frac{I_{\rm oc}}{I_{\rm c}}\right)\beta\exp\left(\lambda'_2 t\right), \end{aligned} \tag{20}$$

with α, β representing arbitrary linear combination coefficients. The decay times of the two solutions are equal, respectively, to

$$\tau_1 = \frac{I_{\rm c}}{{\rm Re}\,\gamma_b}\,, \tag{21}$$

$$\tau_2 = \frac{I_{\rm oc} I_{\rm ic}}{I_{\rm c}\,{\rm Re}\,\gamma_a + I_{\rm ic}\,{\rm Re}\,\gamma_b}\,, \tag{22}$$

where

$${\rm Re}\,\gamma_a = \pi\rho_0(a)a^4\sqrt{\nu_a\Omega}\,\frac{\sqrt{2}}{35}\left(9\sqrt{3}+19\right), \tag{23}$$

$${\rm Re}\,\gamma_b = \pi\rho_0(b)b^4\sqrt{\nu_b\Omega}\,\frac{\sqrt{2}}{35}\left(9\sqrt{3}+19\right). \tag{24}$$

Again, correct to first order in the small quantity γ_b/γ_a, the ratio of the decay times takes the form

$$\frac{\tau_2}{\tau_1} = \frac{I_{\rm oc} I_{\rm ic}}{I_{\rm c}^2}\,\frac{{\rm Re}\,\gamma_b}{{\rm Re}\,\gamma_a} = \frac{I_{\rm oc} I_{\rm ic}}{I_{\rm c}^2}\,\frac{\gamma_b}{\gamma_a}\,. \tag{25}$$

With $I_{\rm oc} = 911.79 \times 10^{34}$ kg m^2, $I_{\rm ic} = 6.16 \times 10^{34}$ kg m^2, and, hence, $I_{\rm c} = 917.95 \times 10^{34}$ kg m^2, we obtain $\tau_2/\tau_1 = 1/17{,}613$. Thus, the second solution damps out rapidly, and we are left with the relationships

$$C = \left(1 + \frac{\gamma_b}{\gamma_a}\,\frac{I_{\rm ic}}{I_{\rm c}}\right)B\,, \tag{26}$$

$$B - C = -\frac{\gamma_b}{\gamma_a}\,\frac{I_{\rm ic}}{I_{\rm c}}\,B\,. \tag{27}$$

From expression (85) it follows that the total rate of energy dissipation at both boundaries becomes

$$\frac{{\rm d}E}{{\rm d}t} = \pi\rho_0(b)A_b^2 b^4\sqrt{\nu_b\Omega}\,\frac{\sqrt{2}}{35}\left(9\sqrt{3}+19\right)\left[1 + \frac{\gamma_b}{\gamma_a}\left(\frac{I_{\rm ic}}{I_{\rm c}}\right)^2\right]. \tag{28}$$

The energy dissipated per cycle is given by

$$\begin{aligned} E &= \frac{2\pi}{\Omega}\,\frac{{\rm d}E}{{\rm d}t} = \frac{2}{35}\,\pi^2\rho_0(b)A_b^2 b^4\sqrt{\frac{2\nu_b}{\Omega}}\left(9\sqrt{3}+19\right)\\ &\quad\times\left[1 + \frac{\gamma_b}{\gamma_a}\left(\frac{I_{\rm ic}}{I_{\rm c}}\right)^2\right]. \end{aligned} \tag{29}$$

The total energy of the motion is written out as

$$T = \frac{1}{2}\, I_{\rm oc} A_b^2 + \frac{1}{2}\, I_{\rm ic}\left(1 + \frac{\gamma_b}{\gamma_a}\,\frac{I_{\rm ic}}{I_{\rm c}}\right)^2 = \frac{1}{2}\, I_{\rm c}\left[1 + 2\,\frac{\gamma_b}{\gamma_a}\left(\frac{I_{\rm ic}}{I_{\rm c}}\right)^2\right]A_b^2 \tag{30}$$

to first order in the small quantity γ_b/γ_a. To the same order, the wobble quality factor can be written in the form

$$Q_{\rm W} = \frac{2\pi T}{E} = \frac{35 I_{\rm c}\left[1+\gamma_b/\gamma_a (I_{\rm ic}/I_{\rm c})^2\right]}{2\pi\rho_0(b) b^4 \sqrt{2\nu_b/\Omega}\left(9\sqrt{3}+19\right)} . \qquad (31)$$

Finally, correct to first order in the ratio γ_b/γ_a, the viscosity recovered from the observed $Q_{\rm W}$ of the nearly diurnal retrograde wobbles equals

$$\nu_b = \frac{1225 I_{\rm c}^2 \Omega\left[1+2\gamma_b/\gamma_a (I_{\rm ic}/I_{\rm c})^2\right]}{8\pi^2 \rho_0^2(b) b^8 \left(9\sqrt{3}+19\right)^2 Q_{\rm W}^2} . \qquad (32)$$

We see from this expression that the inner core is tightly coupled to the outer core and its motion, and that the correction for dissipation in the lower boundary layer, represented by the quantity in square brackets in the numerator, differs from unity by only 3.8×10^{-7} and may be neglected.

Using expression (32) and the values of $Q_{\rm W}$ listed in Table 1, we recover a viscosity of 3038 ± 1362 Pa s for the RFCN from the GSFC series, 2866 ± 1203 Pa s from the USNO series, 2129 ± 2157 Pa s for the PFCN from the GSFC series, and 1452 ± 1396 Pa s from the USNO series. The mean value of the recovered dynamic viscosity reaches then 2371 ± 1530 Pa s. For a density of 9.82×10^3 kg m^{-3} at the top of the core, the corresponding kinematic viscosity is 0.2414 ± 0.1558 m^2 s^{-1}.

3. Viscosity at the bottom of the outer core

Near the bottom of the outer core, the viscosity in the F-layer [46, 47] can be found from the reduction in the rotational splitting of the two equatorial translational modes of the inner core. The translational modes are observed in the so-called Product Spectrum of global networks of superconducting gravimeters [41–43]. Figure 3 demonstrates the three translational mode resonances found in the Product Spectrum, based on the observations at Bad Homburg (24,272 hours), Brussels (83,892 hours), Cantley (32,992 hours), and Strasbourg (78,504 hours). Both the prograde and axial mode resonances are determined with probability well above 95% C.I. and the retrograde mode is just below this level of significance (see Fig. 8(b) in Ref. [44]).

A much more stringent test of significance arises from consideration of the pressure and viscous drags on the inner core [47], which leads to a splitting law in the form

$$\left(\frac{T}{T_0}\right)^2 + 2g^{\nu}\,\frac{T_0}{T_{\rm s}}\left(\frac{T}{T_0}\right) - 1 = 0 , \qquad (33)$$

where T is the period, T_0 is the unsplit period, $T_{\rm s}$ is the length of the sidereal day, and g^{ν} is a dimensionless viscous splitting parameter. For the axial mode, the viscous splitting parameter is related to the inviscid splitting parameter $g^{\rm i}$ by the expression

$$g^{\nu} = g^{\rm i}\left[1+\frac{1}{4}\,\frac{M_{\rm I}-M_{\rm I}'}{M_{\rm I}+\alpha}\,\sqrt{\rm Ek}\,f^{\rm a}(\sigma)\right] , \qquad (34)$$

and for the equatorial modes by

$$g^{\nu} = g^{\rm i}\left[1-\frac{1}{8}\left(\frac{M_{\rm I}'-\beta}{M_{\rm I}+\beta}+\frac{M_{\rm I}'+\alpha}{M_{\rm I}+\alpha}\right)\sqrt{\rm Ek}\,f^{\rm e}(\sigma)\right] , \qquad (35)$$

where Ek is the Ekman number, α, β are the coefficients of the pressure drag on the inner core given by

$$\alpha = M_{\rm I}'\left(\frac{1}{2}+\frac{3}{2}\,\frac{M_{\rm I}+(a/b)^3 M_{\rm S}}{M_{\rm O}+M_{\rm S}\left(1-(a/b)^3\right)}\right) , \qquad (36)$$

$$\beta = M_{\rm I}'\left(\frac{1}{4}-\frac{3}{4}\,\frac{M_{\rm I}+(a/b)^3 M_{\rm S}}{M_{\rm O}+M_{\rm S}\left(1-(a/b)^3\right)}\right) , \qquad (37)$$

$M_{\rm I}$ is the mass of the inner core, $M_{\rm O}$ is the mass of the outer core, $M_{\rm S}$ is the mass of the shell, and $M_{\rm I}' = 4/3\pi a^3\rho_0(a)$ is the displaced mass, with $\rho_0(a)$ being the density at the bottom of the outer core, $\sigma = \omega/2\Omega$ is the dimensionless Coriolis frequency corresponding to angular frequency ω, and, finally, $f^{\rm a}(\sigma)$, $f^{\rm e}(\sigma)$ are dimensionless functions of σ defined as

$$f^{\rm a}(\sigma) = \left\{8\left[(\sigma+1)^{3/2}+(\sigma-1)^{3/2}\right] - \frac{16}{5}\left[(\sigma+1)^{5/2}-(\sigma-1)^{5/2}\right]\right\} , \qquad (38)$$

$$f^{\rm e}(\sigma) = \left\{\mp24(\pm\sigma\mp1)^{1/2} - 16(\pm\sigma\mp1)^{3/2} - \frac{16}{5}\left[(\pm\sigma-1)^{5/2}-(\pm\sigma+1)^{5/2}\right]\right\} , \qquad (39)$$

with the upper sign referring to the retrograde mode, for which σ is positive, and the lower sign referring to the prograde mode, for which σ is negative.

For three candidate periods, namely $T_{\rm R}$ (retrograde), $T_{\rm C}$ (axial) and $T_{\rm P}$ (prograde), the splitting equation (33) provides the corresponding values of the dimensionless viscous splitting parameter, $g_{\rm R}^{\nu}$, $g_{\rm C}^{\nu}$, and $g_{\rm P}^{\nu}$, for a given value of T_0. Thus, the whole frequency axis can be searched for correctly

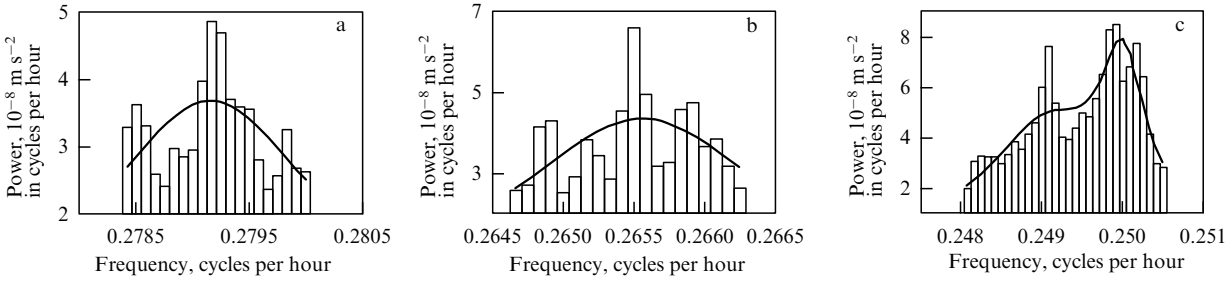

Figure 3. Product Spectra of the retrograde equatorial (a), axial (b), and prograde equatorial (c) translational modes of the inner core. The prograde equatorial mode is near the large solar heating tide feature S_6 at exactly six cycles per solar day. The recovered central periods are equal, respectively, to 3.5822 ± 0.0012 h, 3.7656 ± 0.0015 h, and 4.0150 ± 0.0010 h.

split resonances. For a resonance centered at frequency f_j, its form at neighboring frequencies f_i is given by

$$r_{ij} = \frac{a_j^2}{1 + 4Q\left[(f_i - f_j)/f_j\right]^2}\,. \tag{40}$$

For record segments of 12,000 hours in length, Product Spectrum estimates s_i are spaced at $1/12,000$ cycles/hour intervals along the frequency axis. In the subtidal band, between the 2 h and 8 h periods, there are 4501 spectral estimates. For twenty-five spectral estimates centered at frequency f_j with $Q = 100$, the misfit (40) to spectral estimate s_i is expressed as

$$\varepsilon_{ij} = A_j r_{ij} - s_i\,. \tag{41}$$

The error energy of the fit is written out as

$$I_j = \sum_{i=j-12}^{j+12} \varepsilon_{ij}^2\,. \tag{42}$$

Minimizing the error energy of the fit gives

$$A_j = \frac{\sum_{i=j-12}^{j+12} r_{ij} s_i}{\sum_{i=j-12}^{j+12} r_{ij}^2} \tag{43}$$

with the minimum error energy

$$I_{\min} = \sum_{i=j-12}^{j+12} s_i^2 - A_j^2 \sum_{i=j-12}^{j+12} r_{ij}^2\,. \tag{44}$$

As a measure of the strength of a potential resonance of the form (40), we use the parameter $S_j^2 = A_j^2/I_{\min}$. When a large well-fit resonance is found, we expect S_j^2 to be large, and if a small, poorly fit spectral feature is found, we expect S_j^2 to be small. For each of the available 4477 frequencies f_j in the subtidal band, we set $T_0 = 1/f_j$ and compute $f_R = 1/T_R$, $f_C = 1/T_C$, and $f_P = -1/T_P$ from equation (33). The values of S_R^2, S_C^2, and S_P^2 of the resonance parameter S^2 at the discrete frequencies nearest to f_R, f_C, and f_P, respectively, are then multiplied together to form the splitting product P_j as an indicator of the presence of correctly split resonances. We show in Fig. 4 the resulting probability density function (PDF) for the splitting product computed at 4119 points along the frequency axis in the subtidal band.

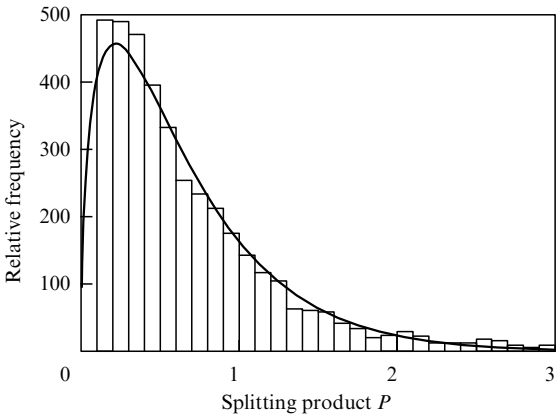

Figure 4. Probability density function (PDF) for the splitting product P. Bins in P are 0.1 wide. The fitted PDF is for a χ_ν^2 distribution with $\nu = 2.97614$ for the random variable 4.5314 P.

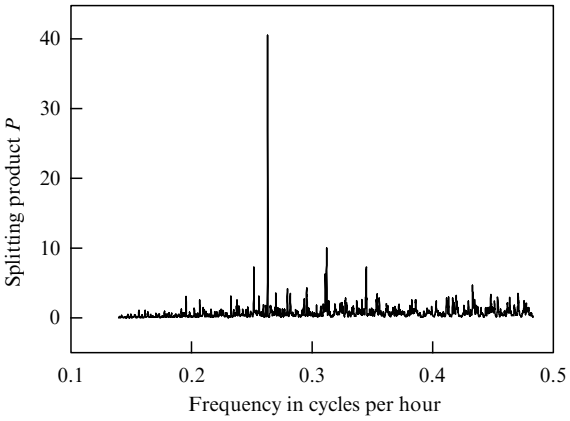

Figure 5. Splitting product P as a function of frequency. The large spike at $T_0 = 3.7975$ corresponds to the translational triplet plotted in Fig. 3.

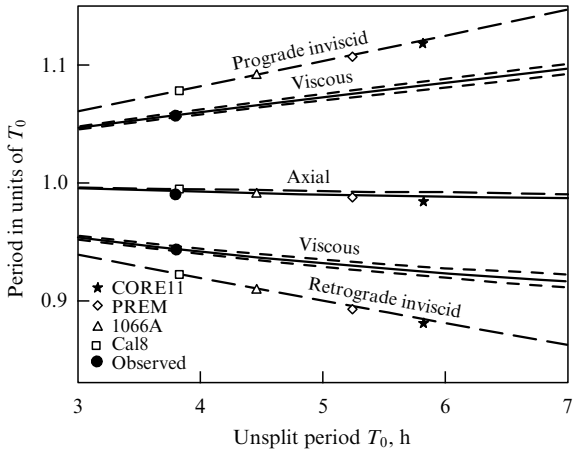

Figure 6. Splitting curves for the three translational modes. The inviscid curves are shown dashed using the splitting parameters for Earth model Cal8 (squares) of Bolt and Urhammer (see Ref. [20] and Appendix A). Inviscid periods are also plotted for the Earth models Core11 (stars) [48], PREM (diamonds) [49] and 1066A (triangles) [50]. Solid viscous splitting curves are for a single viscosity of 1.247×10^{11} Pa s.

Table 2. Inviscid periods for the four Earth models shown plotted in Fig. 6.

Periods	Retrograde, h	Axial, h	Prograde, h
Core11	5.1280	5.7412	6.5114
PREM	4.6776	5.1814	5.7991
1066A	4.0491	4.4199	4.8603
Cal8	3.5168	3.7926	4.1118

The PDF plotted in Fig. 4 allows the evaluation of the significance of translational triplets along the frequency axis. In Fig. 5 we present the splitting products found between 2 h and 10 h periods. A very large value of P is found at $T_0 = 3.7975$ h. From the PDF it is deduced that the probability of a realization of P_j larger than the largest value shown in Fig. 5 is only 1 in 6.8×10^{38}! The resonances shown in Fig. 3 seem to have been correctly identified as translational modes.

Plots of the splitting law for the three translational modes are shown in Fig. 6. The inviscid periods for the four Earth models plotted in this figure are listed in Table 2.

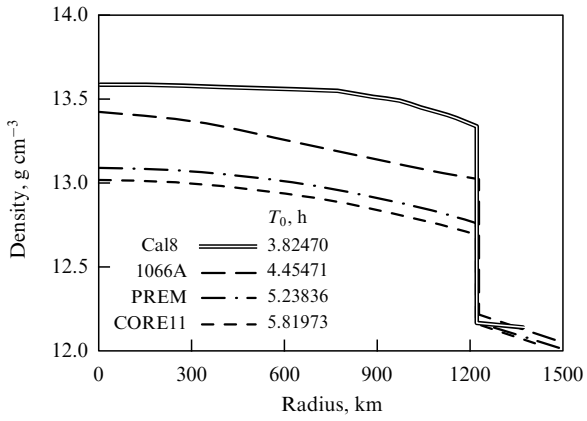

Figure 7. Detailed density profiles of the inner core for Earth models Cal8, 1066A, PREM, and Core11. The scatter of 0.6 g cm^{-3} causes a nearly 2 h difference in the unsplit period T_0, giving a resolution of 200 min g^{-1} cm^{-3}.

Table 3. Comparison of the observed translational mode periods with those of the Cal8 Earth model.

Periods	Retrograde, h	Axial, h	Prograde, h
Observed	3.5822	3.7656	4.0150
Cal8 Viscous	3.5840	3.7731	4.0168
Cal8 Inviscid	3.5168	3.7926	4.1118

Table 4. Comparison of the unsplit period T_0 for four Earth models with its observed value.

Earth model	Unsplit period T_0, h	Deviation ΔT_0, h	Error, %
Observed	3.7985		
Cal8	3.82470	0.0262	0.69
1066A	4.45471	0.65621	17.28
PREM	5.23836	1.43986	37.91
Core11	5.81973	2.02123	53.21

Two independent measures of viscosity are given, as the reduction in rotational splitting is larger for the retrograde equatorial mode than for the prograde equatorial mode. The retrograde equatorial mode gives the viscosity of $1.190 \pm 0.035 \times 10^{11}$ Pa s, while the prograde equatorial mode gives $1.304 \pm 0.034 \times 10^{11}$ Pa s. An error-balanced value of 1.247×10^{11} Pa s yields viscous periods that are only 6.5 s longer than the observed periods.

From Fig. 6 it follows that the observed periods are closest to those for the Cal8 Earth model. A detailed comparison of the Cal8 periods and those observed is drawn in Table 3.

The close match of the observed periods to those of the Cal8 Earth model is due to the sensitivity of the translational mode periods to inner core density. Figure 7 illustrates the density profiles of the inner core for Earth models Cal8, 1066A, preliminary reference Earth model (PREM), and Core11 together with their unsplit periods T_0.

The axial mode period suffers little rotational or viscous splitting. Its observed period imposes a strict constraint on inner core density. The calculated axial mode period for Cal8 is only 27 s longer than the observed period. An overall density decrease in the inner core of only 2.25 kg m^{-3} would bring them into coincidence, giving a very strong confirmation of Cal8. In Table 4 we make a comparison of the unsplit period T_0 for the four Earth models with the observed value.

The close confirmation of the Cal8 Earth model by the observed axial translational mode period of the inner core raises questions about the differences in the density jump at the ICB among the various Earth models illustrated in Fig. 7. The Cal8 density jump of 1170 kg m^{-3} needs to be reduced by 2.25 kg m^{-3} to 1167.75 kg m^{-3} to bring the axial mode period into coincidence with the observed axial mode period. With a resolution of 0.2 min kg^{-1} m^{-3} in average inner core density, the translational mode periods are very sensitive to density. The dispersion in density jumps among the various Earth models, determined by free oscillation and other seismological observations, suggests that these observations are much less sensitive to inner core density than the translational modes. In fact, the Cal8 Earth model developed by Bolt and Urhammer [51, 52] is in agreement with similar seismological data sets as the other three models.

4. A viscosity profile for the outer core

The boundary values of viscosity we have found are in very close agreement with an Arrhenius extrapolation of laboratory experiments [15, 16], giving 10^{11} Pa s at the bottom of the outer core, and 10^2 Pa s at the top. Although the uncertainties in such extrapolations are very large, we are prompted by their close agreement with the measured values to apply the Arrhenius model to interpolation between the boundary values, thus obtaining a viscosity profile across the entire outer liquid core [53].

The Arrhenius description of the temperature and pressure dependence of the dynamic viscosity η is the following [15]:

$$\eta \sim \exp \frac{E_{\mathrm{act}_0} + PV_{\mathrm{act}}}{kT}, \tag{45}$$

with E_{act_0} representing the activation energy at normal pressure, P the pressure, V_{act} the activation volume, k Boltzmann's constant, and T the temperature in kelvins. V_{act} is proportional to the atomic volume V_{at} which, in turn, is inversely proportional to the density ρ. While the activation volume for liquid metals at atmospheric pressure is very small [8, 9], it was supposed [15, 16] that, similar to the behavior of molecular melts, the activation volume in liquid metals increases under compression from $0.05\,V_{\mathrm{at}}$ to $(0.2-0.4)\,V_{\mathrm{at}}$ at pressures of ≈ 10 GPa and can increase further to $(0.5-1)\,V_{\mathrm{at}}$ with a subsequent pressure rise to 100 GPa. The strong pressure dependence requires integration of the differential form of the Arrhenius expression. For dominant pressure dependence, from expression (45) it follows that the differential increment in viscosity is proportional to

$$\frac{E}{\rho T_{\mathrm{m}}} \exp\left(E\,\frac{P}{\rho T_{\mathrm{m}}}\right) \mathrm{d}P, \tag{46}$$

with E being a pressure-dependent parameter allowing for the pressure dependence of the activation volume, T_{m} the melting temperature, and $\mathrm{d}P$ being the differential increment in pressure. The integral of expression (46) over pressure is easily converted to an integral over radius r since $\mathrm{d}P/\mathrm{d}r = -\rho g$, where g is the gravitational acceleration directed toward the center of the Earth. The viscosity at radius r is then

$$\eta(r) = \eta_b + \eta_b \int_b^r \frac{E}{\rho T_{\mathrm{m}}} \exp\left(E\,\frac{P}{\rho T_{\mathrm{m}}}\right) \frac{\mathrm{d}P}{\mathrm{d}r}\,\mathrm{d}r, \tag{47}$$

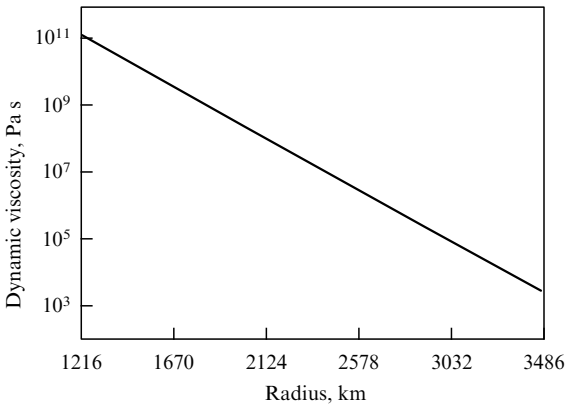

Figure 8. Viscosity profile for Earth's outer core.

Table 5. Pressure, density, melting temperature, and radial pressure gradient profiles.

Radius, km	P, 10^{11} Pa	ρ, 10^3 kg m^{-3}	T_m, K	dP/dr, 10^4 Pa m^{-1}
1216	3.300	12.20	4961	−5.600
1371	3.223	12.14	4905	−6.094
1571	3.094	12.03	4824	−6.737
1821	2.916	11.84	4710	−7.507
2171	2.636	11.52	4521	−8.479
2571	2.278	11.11	4258	−9.421
2971	1.886	10.62	3936	−10.12
3171	1.681	10.33	3751	−10.34
3371	1.473	10.01	3551	−10.47
3486	1.350	9.860	3429	−10.56

where b is the radius of the core–mantle boundary, and $\eta_b = 2371$ Pa s is the dynamic viscosity at the top of the core. To perform the integration in formula (47), we require profiles of pressure, density, melting temperature, and pressure gradient. The pressure profile can be found by integrating the product of gravity and density for an Earth model (here we use Cal8, see Bullen and Bolt [20, pp. 472–473]). The melting temperatures are found by spline interpolation onto the Cal8 radii from those tabulated by Stacey [54, p. 459]. The required profiles are accumulated in Table 5.

Since the activation volume increases strongly with pressure [15, 16], as represented by our parameter E in formula (46), we allow for a linear variation with depth through

$$E = E_b + \frac{b-r}{b-a}\,E_a\,, \tag{48}$$

where a is the radius of the inner core, and E_b, E_a are the constants. The integration in Eqn (47) is carried out by Simpson's rule over 100 steps with spline interpolation across the whole outer core. It turns out that the constant E_b controls the curvature of the viscosity profile near the core–mantle boundary, while the curvature otherwise departs only slightly from log-linear. Some numerical experimentation shows that the viscosity profile is closely log-linear, even near the core–mantle boundary, for a value of $E_b = 4.5 \times 10^{-4}$ m^{-2} s^2 K and that for $E_a = 2.976 \times 10^{-3}$ m^{-2} s^2 K the viscosity at the bottom of the outer core, $\eta_a = 1.247 \times 10^{11}$ Pa s, is closely matched. The resulting viscosity profile is plotted in Fig. 8.

5. Conclusion

Given past discrepancies, the agreement between outer core viscosities measured from VLBI observations of nutations, superconducting gravimeter observations of translational modes, and Arrhenius extrapolation of laboratory high-pressure and high-temperature experiments is quite remarkable. The very large gap between direct observations and extrapolations of laboratory values appears to have closed. Nonetheless, there have been several investigations using computer simulations and a variety of empirical approaches [4–13] giving very different values for the viscosity under Earth's core conditions. In addition, our interpolation of viscosity between the boundary values was carried out along the melting temperature curve rather than along the actual geotherm. It should be noted that the majority of experiments [8–11] performed up to the present point to an insignificant viscosity increase in iron-based melts under pressure with the appropriate activation volume $V_{act} \approx 0.1\,V_{at}$. However, the narrow ranges of viscosity variations in melts that have been studied does not allow a particular model to be chosen for the extrapolation of the viscosity to the megabar range of outer core pressures (135–330 GPa). For example, Dobson [13] showed that different analytic equations which closely describe the observed pressure dependences of material properties give strikingly different extrapolation results. Thus, the Arrhenius and free volume models employed in the extrapolation of iron melt viscosity to the pressures of 135 to 330 GPa existing in the outer core of the Earth give diffusivities that differ by 10 orders of magnitude, as illustrated in Fig. 9.

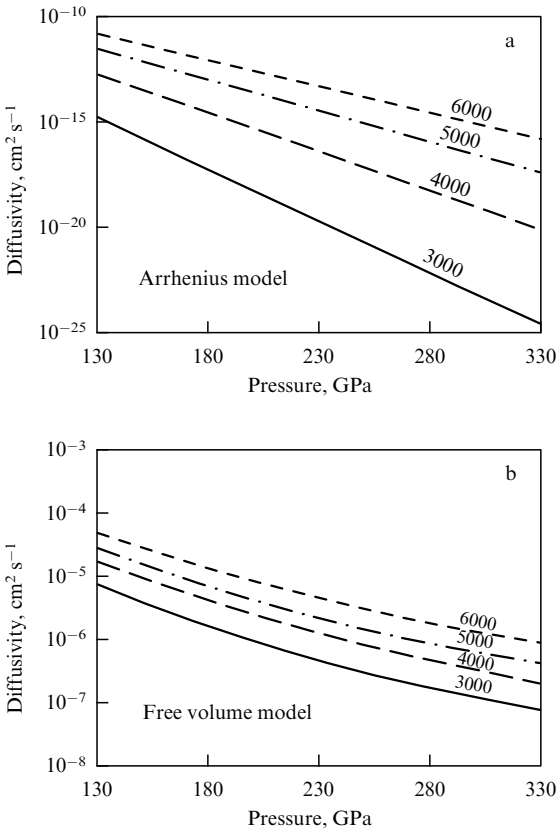

Figure 9. Differences in extrapolations of diffusivities by the Arrhenius (a) and free volume (b) models for temperatures of 3000, 4000, 5000, and 6000 K. (Reproduced from Dobson [13].)

As discussed in review [16], the dynamic viscosity at its low magnitudes is inversely proportional to the diffusivity by the Stokes – Einstein relation (see Ref. [13, Eqn (13)]), but at higher viscosities one finds $D \sim \eta^{-\alpha}$ with α in the range of 0.28 to 0.75. The large uncertainties, as well as the impossibility of reliable extrapolation of the viscosity data obtained at pressures of less than 10 GPa to the megabar range, were also discussed in the review [55]. References [15, 16] presented arguments in support of the Arrhenius model and the rapid activation volume increase with pressures in the 135 to 330 GPa range. There are several theoretical estimates [4 – 7] which give only a minor increase in the iron melt viscosity under pressure. However, the same theoretical computations [56] revealed the iron melting temperature in the megabar range to be widely different from the one found experimentally [57]. It is possible that the calculations do not adequately account for the behavior of iron's inner electron shell at superhigh pressures. Apparently, some new investigations, both experimental and theoretical, are urgently needed, while the data presented in this paper allow us to conclude that the very high viscosity found for iron-based melts in the Earth's outer core is highly probable.

The viscosity values involved are appropriate for molecular viscosities and they are large enough to ensure that flows in the core remain laminar, in contradiction to conventional thought that the flows are turbulent and that the larger viscosities reflect eddy viscosities.

According to the viscosity profile we have derived, the local Ekman number ranges from 1.2×10^{-2} at the bottom to 2.7×10^{-10} at the top of the outer core. Our results appear to confirm the hypothesis advanced by Braginsky [58] that the release of the latent heat of fusion as metallic constituents freeze out in the F-layer at the bottom of the outer core may be the energy source required to drive the geodynamo through compositional convection as studied by Loper and Roberts [59]. At the same time, except in the very lower part of the outer core, Ekman numbers fall in the range of 10^{-4} to 10^{-5}, or even less, thus satisfying the conditions in which numerical dynamos operate [60].

Hence, both laboratory measurements and direct observations imply quite high viscosities in Earth's outer core, apparently confirming the strong pressure dependence of the activation volume found experimentally [15, 16]. It is no longer necessary to invoke turbulent flows and large eddy viscosities for explaining the gap between extrapolations of laboratory measurements and directly observed viscosities of the outer core.

Acknowledgments
D.E.S. is grateful for financial support from the Natural Sciences and Engineering Research Council of Canada. We are indebted to Keith Aldridge for bringing the intricacies of Ekman layer theory to our attention.

6. Appendices

A. Ekman boundary layers and dissipation

In this Appendix, we describe in detail the solution of the boundary layer equations (7) and the calculation of the rates of energy dissipation in the two boundary layers at the boundaries of the outer core. For convenience in keeping track of phase, the velocity components (v_θ, v_ϕ) will be taken to be complex phasors with time and longitude variations given by $\exp\left[-\mathrm{i}(\phi + \Omega t)\right]$. For an assumed radial dependence proportional to $\exp(\lambda r)$, we are led to the homogeneous system of equations

$$\begin{pmatrix} \lambda^2 v + \mathrm{i}\Omega & 2\Omega\cos\theta \\ -2\Omega\cos\theta & \lambda^2 v + \mathrm{i}\Omega \end{pmatrix} \begin{pmatrix} v_\theta \\ v_\phi \end{pmatrix} = 0\,. \tag{49}$$

For this system to have a solution, λ must satisfy the relationship

$$(\lambda^2 v + \mathrm{i}\Omega)^2 = -4\Omega^2\cos^2\theta\,, \tag{50}$$

which is equivalent to

$$\lambda^2 v + \mathrm{i}\Omega = \pm\mathrm{i}2\Omega\cos\theta\,. \tag{51}$$

Substitution of relationship (51) into the system of equations (49) gives

$$v_\phi = \mp\mathrm{i}v_\theta\,, \tag{52}$$

$$v_\phi = \pm\mathrm{i}v_\phi\,. \tag{53}$$

The boundary layers are characterized by the dimensionless Ekman number

$$\mathrm{Ek} = \frac{\nu}{b^2\Omega}\,, \tag{54}$$

with the length scale fixed by the radius b of the CMB. The four roots of the secular equation (50) are $\pm\lambda_1$, $\pm\lambda_2$ with

$$\lambda_1 = \begin{cases} \dfrac{1-\mathrm{i}}{b}\sqrt{\dfrac{1/2+\cos\theta}{\mathrm{Ek}}} = \dfrac{1-\mathrm{i}}{\delta_1} & \text{for} \quad \theta < \dfrac{2\pi}{3}\,, \quad (55) \\ \dfrac{1+\mathrm{i}}{b}\sqrt{\dfrac{-1/2-\cos\theta}{\mathrm{Ek}}} = \dfrac{1+\mathrm{i}}{\delta_1} & \text{for} \quad \theta > \dfrac{2\pi}{3}\,, \quad (56) \end{cases}$$

$$\lambda_2 = \begin{cases} \dfrac{1-\mathrm{i}}{b}\sqrt{\dfrac{1/2-\cos\theta}{\mathrm{Ek}}} = \dfrac{1-\mathrm{i}}{\delta_2} & \text{for} \quad \theta > \dfrac{\pi}{3}\,, \quad (57) \\ \dfrac{1+\mathrm{i}}{b}\sqrt{\dfrac{-1/2+\cos\theta}{\mathrm{Ek}}} = \dfrac{1+\mathrm{i}}{\delta_2} & \text{for} \quad \theta < \dfrac{\pi}{3}\,, \quad (58) \end{cases}$$

with δ_1, δ_2 being the respective boundary layer thicknesses, both of big $O\left(\sqrt{\mathrm{Ek}}\right)$.

In the boundary layer near the top of the core, the perturbing velocity components (v_θ, v_ϕ) vanish with decreasing radius and increase with elevation of radius, so that at $r = b$ they are equal and opposite in sign to the interior nutation velocity components (6), thus satisfying the no-slip condition at the CMB. Hence, the admissible values of λ satisfying equation (51) are λ_1, λ_2. In the boundary layer near the bottom of the outer core, the perturbing velocity components vanish with increasing radius and increase with decreasing radius, thus satisfying the no-slip condition at the ICB. There, the admissible values of λ satisfying equation (51) are $-\lambda_1$, $-\lambda_2$. The perturbing velocity components are then given by the linear combinations

$$v_\theta = \exp\left(-\frac{\Delta r}{\delta_1}\right) f \exp\left[\mathrm{i}\left(\frac{\Delta r}{\delta_1} \pm \phi \pm \Omega t\right)\right] + \exp\left(-\frac{\Delta r}{\delta_2}\right) g \exp\left[\mathrm{i}\left(\frac{\Delta r}{\delta_2} \pm \phi \pm \Omega t\right)\right], \tag{59}$$

$$v_\phi = \exp\left(-\frac{\Delta r}{\delta_1}\right) \mathrm{i} f \exp\left[\mathrm{i}\left(\frac{\Delta r}{\delta_1} \pm \phi \pm \Omega t\right)\right] - \exp\left(-\frac{\Delta r}{\delta_2}\right) \mathrm{i} g \exp\left[\mathrm{i}\left(\frac{\Delta r}{\delta_2} \pm \phi \pm \Omega t\right)\right], \tag{60}$$

where the lower signs apply to the range $\pi/3 < \theta < 2\pi/3$, while the upper signs apply to the range $0 < \theta < \pi/3$ for terms involving δ_2, and to the range $2\pi/3 < \theta < \pi$ for terms involving δ_1; Δr is the increment in radius. At the top of the core, one has $\Delta r = b - r$, and at the bottom of the outer core $\Delta r = r - a$. In general, the linear combination coefficients f and g are complex, with real and imaginary parts expressed by

$$f = \alpha + \mathrm{i}\beta\,, \tag{61}$$

$$g = \gamma + \mathrm{i}\varepsilon\,. \tag{62}$$

Both the real and imaginary parts of expressions (59) and (60) are solutions to the boundary layer equations (7). Our interest is in the real parts of the velocity components given by

$$\begin{aligned}\mathrm{Re}\, v_\theta = {} & \exp\left(-\frac{\Delta r}{\delta_1}\right)\left[\left(\alpha\cos\frac{\Delta r}{\delta_1} \pm \beta\sin\frac{\Delta r}{\delta_1}\right)\cos(\phi+\Omega t)\right.\\ & \left.+\left(\beta\cos\frac{\Delta r}{\delta_1} \mp \alpha\sin\frac{\Delta r}{\delta_1}\right)\sin(\phi+\Omega t)\right]\\ & +\exp\left(-\frac{\Delta r}{\delta_2}\right)\left[\left(\gamma\cos\frac{\Delta r}{\delta_2} \pm \varepsilon\sin\frac{\Delta r}{\delta_2}\right)\cos(\phi+\Omega t)\right.\\ & \left.+\left(\varepsilon\cos\frac{\Delta r}{\delta_2} \mp \gamma\sin\frac{\Delta r}{\delta_2}\right)\sin(\phi+\Omega t)\right], \end{aligned}\tag{63}$$

$$\begin{aligned}\mathrm{Re}\, v_\phi = {} & \exp\left(-\frac{\Delta r}{\delta_1}\right)\left[\left(-\beta\cos\frac{\Delta r}{\delta_1} \pm \alpha\sin\frac{\Delta r}{\delta_1}\right)\cos(\phi+\Omega t)\right.\\ & \left.+\left(\alpha\cos\frac{\Delta r}{\delta_1} \pm \beta\sin\frac{\Delta r}{\delta_1}\right)\sin(\phi+\Omega t)\right]\\ & +\exp\left(-\frac{\Delta r}{\delta_2}\right)\left[\left(\varepsilon\cos\frac{\Delta r}{\delta_2} \mp \gamma\sin\frac{\Delta r}{\delta_2}\right)\cos(\phi+\Omega t)\right.\\ & \left.+\left(-\gamma\cos\frac{\Delta r}{\delta_2} \mp \varepsilon\sin\frac{\Delta r}{\delta_2}\right)\sin(\phi+\Omega t)\right]. \end{aligned}\tag{64}$$

For velocity components (63) and (64) to cancel the components of velocity (6) at the boundaries, we reduce them to the form

$$\begin{aligned}\mathrm{Re}\, v_\theta &= (\alpha+\gamma)\cos(\phi+\Omega t) + (\beta+\varepsilon)\sin(\phi+\Omega t)\\ &= Ar_0\sin(\phi+\Omega t)\,, \end{aligned}\tag{65}$$

$$\begin{aligned}\mathrm{Re}\, v_\phi &= (\varepsilon-\beta)\cos(\phi+\Omega t) + (\alpha-\gamma)\sin(\phi+\Omega t)\\ &= Ar_0\cos\theta\cos(\phi+\Omega t)\,, \end{aligned}\tag{66}$$

where r_0 is the boundary radius: $r_0 = b$ at the top of the outer core, and $r_0 = a$ at the bottom of the outer core. Then, one obtains

$$\beta = \frac{1}{2}\,Ar_0(1-\cos\theta)\,, \qquad \varepsilon = \frac{1}{2}\,Ar_0(1+\cos\theta)\,,$$
$$\alpha = \gamma = 0\,. \tag{67}$$

Differentiation of expressions (63) and (64) yields the derivatives of the velocity components at the top of the core:

$$\begin{aligned}\frac{\partial \mathrm{Re}\, v_\theta}{\partial r} = {} & \left(\mp\frac{\beta}{\delta_1} \mp \frac{\varepsilon}{\delta_2}\right)\cos(\phi+\Omega t)\\ & +\left(\frac{\beta}{\delta_1}+\frac{\varepsilon}{\delta_2}\right)\sin(\phi+\Omega t)\,, \end{aligned}\tag{68}$$

$$\begin{aligned}\frac{\partial \mathrm{Re}\, v_\phi}{\partial r} = {} & \left(-\frac{\beta}{\delta_1}+\frac{\varepsilon}{\delta_2}\right)\cos(\phi+\Omega t)\\ & +\left(\mp\frac{\beta}{\delta_1} \pm \frac{\varepsilon}{\delta_2}\right)\sin(\phi+\Omega t)\,, \end{aligned}\tag{69}$$

while those at the bottom of the outer core are the negatives of these. At the top of the core, the leading order stresses on the outer surface are equal to

$$\sigma_{r\theta} = \eta\,\frac{\partial \mathrm{Re}\, v_\theta}{\partial r}\,, \qquad \sigma_{r\phi} = \eta\,\frac{\partial \mathrm{Re}\, v_\phi}{\partial r}\,, \tag{70}$$

where η is the dynamic viscosity. At the bottom of the outer core, the leading order stresses on the inner surface are the negatives of these, so that on both core surfaces the rate of energy dissipation per unit area in a motion with velocity (6) directed against these stresses takes the form

$$\begin{aligned}\frac{\mathrm{d}e}{\mathrm{d}r} &= v_\theta\sigma_{r\theta} + v_\phi\sigma_{r\phi}\\ &= Ar_0\eta\left\{\left(\mp\frac{\beta}{\delta_1}\mp\frac{\varepsilon}{\delta_2}\right)\cos(\phi+\Omega t)\sin(\phi+\Omega t)\right.\\ &\quad +\left(\frac{\beta}{\delta_1}+\frac{\varepsilon}{\delta_2}\right)\sin^2(\phi+\Omega t)\\ &\quad +\cos\theta\left[\left(\frac{\varepsilon}{\delta_2}-\frac{\beta}{\delta_1}\right)\cos^2(\phi+\Omega t)\right.\\ &\quad \left.\left.+\left(\mp\frac{\beta}{\delta_1}\pm\frac{\varepsilon}{\delta_2}\right)\cos(\phi+\Omega t)\sin(\phi+\Omega t)\right]\right\}. \end{aligned}\tag{71}$$

Substitution of formulas (55)–(58) and (67) yields the desired result for $0 < \theta < \pi/3$:

$$\begin{aligned}\frac{\mathrm{d}e}{\mathrm{d}t} = {} & \frac{1}{2}\,\rho_0 A^2 r_0^2\left\{\sqrt{\nu\Omega\left(\frac{1}{2}+\cos\theta\right)}\right.\\ & \times\left[\sin^2\theta\big(\cos(\phi+\Omega t)\sin(\phi+\Omega t) - \cos^2(\phi+\Omega t)\big)\right.\\ & \left.+1-\cos\theta\right] - \sqrt{\nu\Omega\left(-\frac{1}{2}+\cos\theta\right)}\\ & \times\left[\sin^2\theta\big(\cos(\phi+\Omega t)\sin(\phi+\Omega t) + \cos^2(\phi+\Omega t)\big)\right.\\ & \left.\left.-1-\cos\theta\right]\right\}, \end{aligned}\tag{72}$$

for $\pi/3 < \theta < 2\pi/3$:

$$\begin{aligned}\frac{\mathrm{d}e}{\mathrm{d}t} = {} & \frac{1}{2}\,\rho_0 A^2 r_0^2\left\{\sqrt{\nu\Omega\left(\frac{1}{2}+\cos\theta\right)}\right.\\ & \times\left[\sin^2\theta\big(\cos(\phi+\Omega t)\sin(\phi+\Omega t) - \cos^2(\phi+\Omega t)\big)\right.\\ & \left.+1-\cos\theta\right] + \sqrt{\nu\Omega\left(\frac{1}{2}-\cos\theta\right)}\\ & \times\left[\sin^2\theta\big(\cos(\phi+\Omega t)\sin(\phi+\Omega t) - \cos^2(\phi+\Omega t)\big)\right.\\ & \left.\left.+1+\cos\theta\right]\right\}, \end{aligned}\tag{73}$$

and for $2\pi/3 < \theta < \pi$:

$$\frac{\mathrm{d}e}{\mathrm{d}t} = \frac{1}{2}\,\rho_0 A^2 r_0^2 \Bigg\{ -\sqrt{v\Omega\left(-\frac{1}{2}-\cos\theta\right)} \times \Big[\sin^2\theta\big(\cos(\phi+\Omega t)\sin(\phi+\Omega t)+\cos^2(\phi+\Omega t)\big) - 1+\cos\theta\Big] + \sqrt{v\Omega\left(\frac{1}{2}-\cos\theta\right)} \times \Big[\sin^2\theta\big(\cos(\phi+\Omega t)\sin(\phi+\Omega t)-\cos^2(\phi+\Omega t)\big) + 1+\cos\theta\Big]\Bigg\}, \tag{74}$$

with ρ_0 standing for the core density just inside the respective boundary.

Integrating over the entire boundary results in the total rate of energy dissipation:

$$\begin{aligned}\frac{\mathrm{d}E}{\mathrm{d}t} &= r_0^2\int_0^{2\pi}\int_0^{\pi}\frac{\mathrm{d}e}{\mathrm{d}t}\sin\theta\,\mathrm{d}\theta\,\mathrm{d}\phi = -\frac{\pi}{2}\,\rho_0 A^2 r_0^4\sqrt{v\Omega} \\ &\times\Bigg\{\int_0^{\pi/3}\sqrt{\frac{1}{2}+\cos\theta}\,\sin\theta(1-\cos\theta+\sin^2\theta)\,\mathrm{d}\theta \\ &+\int_0^{\pi/3}\sqrt{-\frac{1}{2}+\cos\theta}\,\sin\theta(1+\cos\theta+\sin^2\theta)\,\mathrm{d}\theta \\ &+\int_{\pi/3}^{2\pi/3}\sqrt{\frac{1}{2}+\cos\theta}\,\sin\theta(1-\cos\theta+\sin^2\theta)\,\mathrm{d}\theta \\ &+\int_{\pi/3}^{2\pi/3}\sqrt{\frac{1}{2}-\cos\theta}\,\sin\theta(1+\cos\theta+\sin^2\theta)\,\mathrm{d}\theta \\ &+\int_{2\pi/3}^{\pi}\sqrt{-\frac{1}{2}-\cos\theta}\,\sin\theta(1-\cos\theta+\sin^2\theta)\,\mathrm{d}\theta \\ &+\int_{2\pi/3}^{\pi}\sqrt{\frac{1}{2}-\cos\theta}\,\sin\theta(1+\cos\theta+\sin^2\theta)\,\mathrm{d}\theta\Bigg\},\end{aligned} \tag{75}$$

where, in the integration over ϕ, we have made use of the integrals

$$\int_0^{2\pi}\cos(\phi+\Omega t)\sin(\phi+\Omega t)\,\mathrm{d}\phi = \frac{1}{2}\int_0^{2\pi}\sin\big[2(\phi+\Omega t)\big]\,\mathrm{d}\phi = 0\,, \tag{76}$$

$$\int_0^{2\pi}\cos^2(\phi+\Omega t)\,\mathrm{d}\phi = \frac{1}{2}\int_0^{2\pi}\Big\{\cos\big[2(\phi+\Omega t)\big]+1\Big\}\,\mathrm{d}\phi = \pi\,. \tag{77}$$

We may write down expression (75) in the shorthand as

$$\frac{\mathrm{d}E}{\mathrm{d}t} = -\frac{\pi}{2}\,\rho_0 A^2 r_0^4\sqrt{v\Omega}\,[J_1+J_2+J_3+J_4+J_5+J_6]\,, \tag{78}$$

with J_1, J_2, J_3, J_4, J_5, and J_6 representing the six integrals in Eqn (75). Evaluation of the integrals in expression (75) depends on the following indefinite integrals

$$I_1 = \int\left(\frac{s}{2}\mp\cos\theta\right)^{1/2}\sin^3\theta\,\mathrm{d}\theta = \pm\frac{2}{3}\left(\frac{s}{2}\mp\cos\theta\right)^{3/2}\sin^2\theta - \frac{8}{15}\left(\frac{s}{2}\mp\cos\theta\right)^{5/2}\cos\theta\mp\frac{16}{105}\left(\frac{s}{2}\mp\cos\theta\right)^{7/2}, \tag{79}$$

$$I_2 = \int\left(\frac{s}{2}\mp\cos\theta\right)^{1/2}(1-\cos\theta)\sin\theta\,\mathrm{d}\theta = \pm\frac{2}{3}\left(\frac{s}{2}\mp\cos\theta\right)^{3/2}\mp\frac{2}{3}\left(\frac{s}{2}\mp\cos\theta\right)^{3/2}\cos\theta - \frac{4}{15}\left(\frac{s}{2}\mp\cos\theta\right)^{5/2}, \tag{80}$$

$$I_3 = \int\left(\frac{s}{2}\mp\cos\theta\right)^{1/2}(1+\cos\theta)\sin\theta\,\mathrm{d}\theta = \pm\frac{2}{3}\left(\frac{s}{2}\mp\cos\theta\right)^{3/2}\pm\frac{2}{3}\left(\frac{s}{2}\mp\cos\theta\right)^{3/2}\cos\theta + \frac{4}{15}\left(\frac{s}{2}\mp\cos\theta\right)^{5/2}, \tag{81}$$

with s representing the sign, which can take on either the value of $+1$ or the value of -1 throughout each expression. Using formulas (79)–(81), and inserting limits of integration, we arrive at

$$J_1 = \frac{13}{30}+\frac{16}{105}-\frac{18}{35}\sqrt{\frac{3}{2}}\,, \qquad J_2 = -\frac{57}{105}\sqrt{2}\,, \qquad J_3 = -\frac{1}{6}-\frac{44}{105}\,, \tag{82}$$

$$J_4 = -\frac{1}{6}-\frac{44}{105} = J_3\,, \qquad J_5 = -\frac{57}{105}\sqrt{2} = J_2\,, \qquad J_6 = \frac{13}{30}+\frac{16}{105}-\frac{18}{35}\sqrt{\frac{3}{2}} = J_1\,. \tag{83}$$

The six integrals add up to

$$J_1+J_2+J_3+J_4+J_5+J_6 = -2\sqrt{2}\,\frac{9\sqrt{3}+19}{35}\,. \tag{84}$$

Substituting this result into expression (78), we find the rate of energy dissipation in each of the respective boundary layers:

$$\frac{\mathrm{d}E}{\mathrm{d}t} = \frac{\pi}{35}\,\rho_0 A^2 r_0^4\sqrt{2v\Omega}\,\big(9\sqrt{3}+19\big)\,. \tag{85}$$

B. Viscous coupling to the inner core and shell

From relationship (11) it is apparent that the reciprocal of the overall quality factor cannot be less than the reciprocal of the effective quality factor attributed to the boundary layer at the inner core surface. Because of the high viscosity there, the inner core is likely to be tightly coupled to outer core wobbles. The nearly retrograde diurnal wobbles of the outer core, associated with the free core nutations, give rise to viscous torques exerted by the outer core on the inner core and shell.

The viscous torques exerted by the outer core at its boundaries are defined as

$$\boldsymbol{\Gamma} = \int\mathbf{r}\times(\boldsymbol{\theta}\,\sigma_{r\theta}+\boldsymbol{\phi}\,\sigma_{r\phi})\,\mathrm{d}S = \int(-\boldsymbol{\theta}\,r\sigma_{r\phi}+\boldsymbol{\phi}\,r\sigma_{r\theta})\,\mathrm{d}S\,, \tag{86}$$

where the integral is taken over the respective boundary surface. The spherical polar unit vectors are linked to the

Cartesian unit vectors $(\mathbf{i}, \mathbf{j}, \mathbf{k})$ by the relations

$$\boldsymbol{\theta} = \mathbf{i}\cos\theta\cos\phi + \mathbf{j}\cos\theta\sin\phi - \mathbf{k}\sin\theta\,, \tag{87}$$

$$\boldsymbol{\phi} = -\mathbf{i}\sin\phi + \mathbf{j}\cos\phi\,. \tag{88}$$

The Cartesian components of the viscous torques take then the form

$$\begin{aligned}\boldsymbol{\Gamma} &= \mathbf{i}r_0^3\int_0^{2\pi}\int_0^{\pi}\sin\theta(-\sigma_{r\phi}\cos\theta\cos\phi - \sigma_{r\theta}\sin\phi)\,\mathrm{d}\theta\,\mathrm{d}\phi\\ &+ \mathbf{j}r_0^3\int_0^{2\pi}\int_0^{\pi}\sin\theta(-\sigma_{r\phi}\cos\theta\sin\phi + \sigma_{r\theta}\cos\phi)\,\mathrm{d}\theta\,\mathrm{d}\phi\\ &+ \mathbf{k}r_0^3\int_0^{2\pi}\int_0^{\pi}\sigma_{r\phi}\sin^2\theta\,\mathrm{d}\theta\,\mathrm{d}\phi\,.\end{aligned} \tag{89}$$

From expressions (70) for the leading order stresses it is seen that the integrations over ϕ depend on the elementary integrals

$$\begin{aligned}&\int_0^{2\pi}\cos(\phi+\Omega t)\cos\phi\,\mathrm{d}\phi = \pi\cos\Omega t\,,\\ &\int_0^{2\pi}\sin(\phi+\Omega t)\cos\phi\,\mathrm{d}\phi = \pi\sin\Omega t\,,\\ &\int_0^{2\pi}\cos(\phi+\Omega t)\sin\phi\,\mathrm{d}\phi = -\pi\sin\Omega t\,,\\ &\int_0^{2\pi}\sin(\phi+\Omega t)\sin\phi\,\mathrm{d}\phi = \pi\cos\Omega t\,,\\ &\int_0^{2\pi}\cos(\phi+\Omega t)\,\mathrm{d}\phi = \int_0^{2\pi}\sin(\phi+\Omega t)\,\mathrm{d}\phi = 0\,.\end{aligned}$$

The last two integrals ensure that the viscous torques have only equatorial Cartesian components (Γ_x, Γ_y), and writing down $\tilde{\Gamma} = \Gamma_x + \mathrm{i}\Gamma_y$, we arrive at

$$\begin{aligned}\tilde{\Gamma} &= -\pi r_0^3\eta\exp(-\mathrm{i}\Omega t)\int_0^{\pi}\left[\cos\theta\sin\theta\left(\frac{\beta}{\delta_1} - \frac{\varepsilon}{\delta_2}\right)\right.\\ &\left. - \sin\theta\left(\frac{\beta}{\delta_1} + \frac{\varepsilon}{\delta_2}\right)\right]\mathrm{d}\theta\\ &+ \mathrm{i}\pi r_0^3\eta\exp(-\mathrm{i}\Omega t)\int_0^{\pi}\left[\cos\theta\sin\theta\left(\mp\frac{\beta}{\delta_1} \pm \frac{\varepsilon}{\delta_2}\right)\right.\\ &\left. + \sin\theta\left(\pm\frac{\beta}{\delta_1} \pm \frac{\varepsilon}{\delta_2}\right)\right]\mathrm{d}\theta\,.\end{aligned} \tag{90}$$

Substitution of formulas (55)–(58) and (67) testifies that evaluation of the torque expression (90) depends on the integrals

$$\begin{aligned}&\int\sqrt{\frac{s}{2}\mp\cos\theta}\,\cos\theta\sin\theta\,\mathrm{d}\theta\\ &\quad= \pm\frac{2}{3}\cos\theta\left(\frac{s}{2}\mp\cos\theta\right)^{3/2} + \frac{4}{15}\left(\frac{s}{2}\mp\cos\theta\right)^{5/2},\\ &\int\sqrt{\frac{s}{2}\mp\cos\theta}\,\cos^2\theta\sin\theta\,\mathrm{d}\theta\\ &\quad= \pm\frac{2}{3}\left(\frac{s}{2}\mp\cos\theta\right)^{3/2}\cos^2\theta + \frac{8}{15}\left(\frac{s}{2}\mp\cos\theta\right)^{5/2}\cos\theta\\ &\quad\pm\frac{16}{105}\left(\frac{s}{2}\mp\cos\theta\right)^{7/2},\end{aligned}$$

$$\int\sqrt{\frac{s}{2}\mp\cos\theta}\,\sin\theta\,\mathrm{d}\theta = \pm\frac{2}{3}\left(\frac{s}{2}\mp\cos\theta\right)^{3/2}, \tag{91}$$

where, again, s represents the sign which can take on either the value of $+1$ or the value of -1 throughout each expression.

The total viscous torque is made up of contributions from three zones of latitude. The contribution from the region $0 < \theta < \pi/3$ is given by

$$\begin{aligned}\tilde{\Gamma}_{0<\theta<\pi/3} &= -\pi\rho_0 A r_0^4\sqrt{\nu\Omega}\exp(-\mathrm{i}\Omega t)\\ &\times\left\{\frac{41}{140} - \frac{9}{35}\sqrt{\frac{3}{2}} - \frac{19}{35}\frac{1}{\sqrt{2}}\right.\\ &\left. + \mathrm{i}\left[-\frac{41}{140} + \frac{9}{35}\sqrt{\frac{3}{2}} - \frac{19}{35}\frac{1}{\sqrt{2}}\right]\right\},\end{aligned} \tag{92}$$

while the contribution from the region $\pi/3 < \theta < 2\pi/3$ equals

$$\tilde{\Gamma}_{\pi/3<\theta<2\pi/3} = -\pi\rho_0 A r_0^4\sqrt{\nu\Omega}\exp(-\mathrm{i}\Omega t)\,\frac{41}{70}(-1+\mathrm{i})\,, \tag{93}$$

and that from the region $2\pi/3 < \theta < \pi$ is

$$\begin{aligned}\tilde{\Gamma}_{2\pi/3<\theta<\pi} &= -\pi\rho_0 A r_0^4\sqrt{\nu\Omega}\exp(-\mathrm{i}\Omega t)\\ &\times\left\{\frac{41}{140} - \frac{9}{35}\sqrt{\frac{3}{2}} - \frac{19}{35}\frac{1}{\sqrt{2}}\right.\\ &\left. + \mathrm{i}\left[-\frac{41}{140} + \frac{9}{35}\sqrt{\frac{3}{2}} - \frac{19}{35}\frac{1}{\sqrt{2}}\right]\right\}.\end{aligned} \tag{94}$$

The total viscous torque is then defined as

$$\tilde{\Gamma} = \pi\rho_0 A r_0^4\sqrt{\nu\Omega}\exp(-\mathrm{i}\Omega t)\,\frac{19}{35}\sqrt{2}\left[1 + \mathrm{i} + \frac{9}{19}\sqrt{3}\,(1-\mathrm{i})\right]. \tag{95}$$

Separating the torques from the two boundary layers, the outer core exerts the viscous torque

$$\begin{aligned}\tilde{\Gamma}_a &= \pi\rho_0(a)A_a a^4\sqrt{v_a\Omega}\exp(-\mathrm{i}\Omega t)\\ &\times\frac{19}{35}\sqrt{2}\left[1 + \mathrm{i} + \frac{9}{19}\sqrt{3}(1-\mathrm{i})\right]\end{aligned} \tag{96}$$

on the inner core, while it exerts the viscous torque

$$\begin{aligned}\tilde{\Gamma}_b &= \pi\rho_0(b)A_b b^4\sqrt{v_b\Omega}\exp(-\mathrm{i}\Omega t)\\ &\times\frac{19}{35}\sqrt{2}\left[1 + \mathrm{i} + \frac{9}{19}\sqrt{3}(1-\mathrm{i})\right]\end{aligned} \tag{97}$$

on the shell.

The extra nearly diurnal retrograde wobble of the outer core with respect to its boundaries is expressed in complex phasor notation as

$$\tilde{\omega} = \omega_1 + \mathrm{i}\omega_2 = A\exp(-\mathrm{i}\Omega t)\,, \tag{98}$$

with the wobble angular velocity $\boldsymbol{\omega} = (\omega_1, \omega_2)$. The rate at which the outer core does work against the viscous torques is given by

$$\frac{\mathrm{d}E}{\mathrm{d}t} = \boldsymbol{\Gamma}\,\boldsymbol{\omega} = \Gamma_1\omega_1 + \Gamma_2\omega_2 = \frac{1}{2}(\tilde{\omega}\tilde{\Gamma}^* + \tilde{\omega}^*\tilde{\Gamma})\,, \tag{99}$$

where the torque vector is $\mathbf{\Gamma} = (\Gamma_1, \Gamma_2)$ and where the superscript asterisk indicates the complex-conjugate quantity. From the torque equation (95) it follows that the rate of energy dissipation in the boundary layers takes the form

$$\frac{\mathrm{d}E}{\mathrm{d}t} = \frac{\pi}{35}\,\rho_0 A^2 r_0^4 \sqrt{2\nu\Omega}\,\left(9\sqrt{3}+19\right), \tag{100}$$

in agreement with equation (85).

Expressions (96) and (97) for the viscous torques the outer core exerts on its boundaries may be reduced to

$$\tilde{\Gamma}_a = \gamma_a \exp\left(-\mathrm{i}\Omega t\right) A_a\,, \tag{101}$$

$$\tilde{\Gamma}_b = \gamma_b \exp\left(-\mathrm{i}\Omega t\right) A_b\,, \tag{102}$$

where

$$\gamma_a = \pi\rho_0(a) a^4 \sqrt{\nu_a\Omega}\,\frac{19}{35}\,\sqrt{2}\left[1+\mathrm{i}+\frac{9}{19}\,\sqrt{3}\,(1-\mathrm{i})\right], \tag{103}$$

$$\gamma_b = \pi\rho_0(b) b^4 \sqrt{\nu_b\Omega}\,\frac{19}{35}\,\sqrt{2}\left[1+\mathrm{i}+\frac{9}{19}\,\sqrt{3}\,(1-\mathrm{i})\right]. \tag{104}$$

References

1. Lumb L I, Aldridge K D *J. Geomag. Geoelectr.* **43** 93 (1991)
2. Anderson D L *Theory of the Earth* (Boston: Blackwell Sci. Publ., 1989)
3. Davis R G, Whaler K A *Phys. Earth Planet. Inter.* **103** 181 (1997)
4. de Wijs G A et al. *Nature* **392** 805 (1998)
5. Alfè D, Kresse G, Gillan M J *Phys. Rev. B* **61** 132 (2000)
6. Desgrandes C, Delhommelle J *Phys. Rev. B* **76** 172102 (2007)
7. Vočadlo L et al. *Faraday Discuss.* **106** 205 (1997)
8. Rutter M D et al. *Geophys. Res. Lett.* **29** 1217 (2002)
9. Dobson D P et al. *Am. Mineralogist* **85** 1838 (2000)
10. Urakawa S et al. *Am. Mineralogist* **86** 578 (2001)
11. Terasaki H et al. *Geophys. Res. Lett.* **33** L22307 (2006)
12. Rutter M D et al. *Phys. Rev. B* **66** 060102 (2002)
13. Dobson D P *Phys. Earth Planet. Inter.* **130** 271 (2002)
14. Secco R A "Viscosity of the outer core", in *Mineral Physics & Crystallography: A Handbook of Physical Constants* (AGU Reference Shelf, Vol. 2, Ed. T J Ahrens) (Washington, DC: American Geophysical Union, 1995) p. 218
15. Brazhkin V V *Pis'ma Zh. Eksp. Teor. Fiz.* **68** 469 (1998) [*JETP Lett.* **68** 502 (1998)]
16. Brazhkin V V, Lyapin A G *Usp. Fiz. Nauk* **170** 535 (2000) [*Phys. Usp.* **43** 493 (2000)]
17. Poirier J P *Geophys. J.* **92** 99 (1988)
18. Jeffreys H *Mon. Not. R. Astron. Soc. Geophys. Suppl.* **1** 371 (1926)
19. Garland G D *Introduction to Geophysics: Mantle, Core and Crust* (Philadelphia: Saunders, 1971) p. 42
20. Bullen K E, Bolt B A *An Introduction to the Theory of Seismology* 4th ed. (Cambridge: Cambridge Univ. Press, 1985) p. 322
21. Poincaré H *Bull. Astron.* **27** 321 (1910)
22. Aldridge K D "An experimental study of axisymmetric inertial oscillations of a rotating liquid sphere", Ph.D. Thesis (Cambridge, Mass.: MIT, 1967)
23. Smylie D E et al. *Geophys. J. Int.* **108** 465 (1992)
24. Jiang X "Wobble-nutation modes of the Earth", Ph.D. Thesis, (Toronto: York Univ., 1993)
25. Jiang X, Smylie D E *Phys. Earth Planet. Inter.* **90** 91 (1995)
26. Jiang X, Smylie D E *Phys. Earth Planet. Inter.* **94** 159 (1996)
27. Greenspan H P *The Theory of Rotating Fluids* (London: Cambridge Univ. Press, 1968) p. 66
28. Crossley D, Smylie D E *Geophys. J. R. Astron. Soc.* **42** 1011 (1975)
29. Acheson D J *Geophys. J. R. Astron. Soc.* **43** 253 (1975)
30. Smylie D E, Szeto A M K, Rochester M G *Rep. Prog. Phys.* **47** 855 (1984)
31. Smylie D E "Electromagnetic excitation of the Chandler Wobble", Ph.D. Thesis (Toronto: Univ. of Toronto, 1963)
32. Rochester M G, Smylie D E *Geophys. J. Int.* **10** 289 (1965)
33. Buffett B A, Mathews P M, Herring T A *J. Geophys. Res.* **107** (B4) 2070 (2002)
34. Runcorn S K *Trans. Am. Geophys. Union* **36** 191 (1955)
35. Smylie D E *Geophys. J. Int.* **9** 169 (1965)
36. Johnson I M, Smylie D E *Geophys. J. Int.* **22** 41 (1970)
37. Mathews P M et al. *J. Geophys. Res.* **96** (B5) 8219 (1991)
38. de Vries D, Wahr J M *J. Geophys. Res.* **96** (B5) 8275 (1991)
39. Palmer A, Smylie D E *Phys. Earth Planet. Inter.* **148** 285 (2005)
40. Slichter L B *Proc. Natl. Acad. Sci. USA* **47** 186 (1961)
41. Smylie D E et al. *Phys. Earth Planet. Inter.* **80** 135 (1993)
42. Courtier N et al. *Phys. Earth Planet. Inter.* **117** 3 (2000)
43. Smylie D E, Francis O, Merriam J P *J. Geodetic Soc. Jpn.* **47** 364 (2001)
44. Moore D W "Homogeneous fluids in rotation", in *Rotating Fluids in Geophysics* (Eds P H Roberts, A M Soward) (New York: Academic Press, 1978)
45. Smylie D E, McMillan D G *Phys. Earth Planet. Inter.* **117** 71 (2000)
46. Smylie D E *Science* **284** 461 (1999)
47. Smylie D E, McMillan D G *Phys. Earth Planet. Inter.* **117** 71 (2000)
48. Widmer R, Masters G, Gilbert F, in *17th Inter. Conf. on Mathematical Geophysics* (*Blanes, Spain, IUGG, June 1988*)
49. Dziewonski A M, Anderson D L *Phys. Earth Planet. Inter.* **25** 297 (1981)
50. Gilbert F, Dziewonski A M *Philos. Trans. R. Soc. London A* **278** 187 (1975)
51. Bolt B A, Urhammer R *Geophys. J. R. Astron. Soc.* **42** 419 (1975)
52. Bolt B A, Urhammer R A, in *Evolution of the Earth* (Geodynamics Series, Vol. 5, Eds R J O'Connell, W S Fyfe) (Washington, DC: American Geophysical Union, 1981) p. 28
53. Smylie D E, Palmer A, arXiv:0709.3333
54. Stacey F D *Physics of the Earth* 3rd ed. (Brisbane: Brookfield Press, 1992)
55. Mineev V N, Funtikov A I *Usp. Fiz. Nauk* **174** 727 (2004) [*Phys. Usp.* **47** 671 (2004)]
56. Alfe D, Gillan M J, Price G D *Nature* **401** 462 (1999)
57. Boehler R *Nature* **363** 534 (1993)
58. Braginsky S I *Dokl. Akad. Nauk SSSR* **149** 8 (1963)
59. Loper D E, Roberts P H *Phys. Earth Planet. Inter.* **24** 302 (1981)
60. Olson P, Christensen U R *Geophys. J. Int.* **151** 809 (2002)